Journal of Marine Science and Technology

Volume 25 | Issue 5 Article 3

PARAMETRIC STUDY OF PILED-RAFT FOUNDATION IN DEEP EXCAVATION OF TAIPEI METROPOLITAN

Der-Guey Lin
Department of Soil and Water conservation, National Chung-Hsing University, Taichung, Taiwan, R.O.C.

Wei-Hsiang Chen
Department of Soil and Water conservation, National Chung-Hsing University, Taichung, Taiwan, R.O.C.

Wen-Tsung Liu
Department of Civil Engineering, Kao Yuan University, Kaohsiung, Taiwan, R.O.C.

Jui-Ching Chou
Sinotech Engineering Consultants, Taipei, Taiwan, R.O.C., jccchou@mail.sinotech.com.tw

Recommended Citation
Lin, Der-Guey; Chen, Wei-Hsiang; Liu, Wen-Tsung; and Chou, Jui-Ching (2017) "PARAMETRIC STUDY OF PILED-RAFT FOUNDATION IN DEEP EXCAVATION OF TAIPEI METROPOLITAN," *Journal of Marine Science and Technology*: Vol. 25: Iss. 5, Article 3.
DOI: 10.6119/JMST-017-0418-3
Available at: https://jmstt.ntou.edu.tw/journal/vol25/iss5/3

Journal of Marine Science and Technology, Vol. 25, No. 5, pp. 508-519 (2017)
DOI: 10.6119/JMST-017-0418-3

PARAMETRIC STUDY OF PILED-RAFT FOUNDATION IN DEEP EXCAVATION OF TAIPEI METROPOLITAN

Der-Guey Lin[1], Wei-Hsiang Chen[1], Wen-Tsung Liu[2], Jui-Ching Chou[3]

Key words: piled-raft foundation, diaphragm wall, deep excavation, parametric study.

ABSTRACT

The piled-raft foundation has been commonly used in Taipei Metropolitan to solve the low bearing capacity and the excess settlement problem of the raft foundation for the high-rise building. In past studies, effects of the deep excavation, the diaphragm wall and the overburden stress of the surrounding soil on the piled-raft foundation were often ignored in the numerical simulation. In this article, a parametric study on the piled-raft foundation including four influence factors, namely, the shape of the piled-raft foundation, the arrangement of (or the number of) piles in pile group, the length of the pile, and the thickness of the raft, were carried out using three-dimensional finite element method (3-D FEM) to understand their effects on the behaviors of piled-raft foundation. Parametric study results indicate that all four influence factors have significant effects on the settlement of the piled-raft foundation. Other than the settlement, the arrangement of pile has major effects on the pile head loading and the pile bending moment of the piled-raft foundation as well. In addition, the Load Carrying Ratio (*LCR*) of raft in piled-raft foundation is dependent on the raft settlement. A higher *LCR* value is constantly associated with a larger settlement of piled-raft, especially for the piled-raft with a larger *PAF* value (or fewer piles in pile group). Conclusively, the raft carries 20% to 35% of the total vertical load on the piled-raft system of deep excavation in Taipei Metropolitan.

I. INTRODUCTION

During last few decades, the possibility of using a piled-raft foundation to support high-rise buildings as an economical alternative to the conventional piled foundation was gaining popularity in Taipei Metropolitan. The safety and economy of the construction project are then getting more attention. These two objectives can only be satisfied when the load transferring mechanisms between pile, soil and raft are considered in the design or analysis process (Poulos et al., 1997). In order to solve this complex problem, many researchers applied various methods for piled-raft foundations as followed:

(1) Simplified calculation methods-simplifications on modeling the pile, soil and raft interactions (Poulos and Davis, 1980; Randolph, 1983 and Randolph et al., 1994);
(2) Approximate computer-based analyses-using strip on springs approach (Poulos, 1991) or plate on springs approach (Clancy and Randolph, 1993; Poulos, 1994); and
(3) More rigorous computer-based methods-boundary element methods, 3-D FEM (Oh et al., 2009; Lee et al., 2010; Poulos et al., 2011; Karim et al., 2013; Nguyen et al., 2014) or 3-D FDM (three-dimensional finite difference method) (Comodromos et al., 2009).

Based on the previous literatures, it can be concluded that 3-D FEM or 3-D FDM analyses can simulate the actual field conditions better and are recommended to solve the complex problem of the piled-raft foundation. However, effects of the deep excavation, the diaphragm wall and the overburden stress of the surrounding soil on the piled-raft foundation have not been fully investigated in the past.

This article attempts to assess and broaden the understanding of the mechanical behaviors of piled-raft foundation via a parametric study considering the effects of deep excavation, diaphragm wall construction, and overburden stress in a typical Taipei soil profile. Finite element program, PLAXIS 3D, was chosen as the prime numerical tool in this study. Parameters and simulation procedures for the parametric study were first calibrated using pile loading test results in the jobsite of *TIFC* (*T*aipei *I*nternational *F*inancial *C*orporation or *Taipei 101*). PLAXIS 3D is a three-dimensional finite element program, developed for the analysis of deformation, stability and groundwater flow in geotechnical engineering. The development of PLAXIS

Paper submitted 09/25/16; revised 01/16/17; accepted 04/18/17. Author for correspondence: Jui-Ching Chou (e-mail: jccchou@mail.sinotech.com.tw).
[1] *Department of Soil and Water conservation, National Chung-Hsing University, Taichung, Taiwan, R.O.C.*
[2] *Department of Civil Engineering, Kao Yuan University, Kaohsiung, Taiwan, R.O.C.*
[3] *Sinotech Engineering Consultants, Taipei, Taiwan, R.O.C.*

Table 1. Input material model parameters of soil layers and testing pile.

Depth Soil layer (*SPT*)	Cohesion c' (kPa)	Friction angle ϕ' (°)	Poisson's ratio ν'	Young's modulus E' (MPa)	Dry unit weight, γ_d ——— Saturated unit weight, γ_{sat} (kN/m^3)	Dilation angle ψ (°)	R_{inter}
0-2.2 m SF (SPT N = 4-12)	10.0	35	0.30	7.5	17.15 ——— 18.13	5	0.85
2.2-13.4 m CL1a (SPT N = 2-5)	22.5	31	0.30	14.1	18.33 ——— 18.53	0	0.90
13.4-24.5 m CL1b (SPT N = 3-6)	24.0	33	0.30	17.4	18.72 ——— 19.32	0	0.90
24.5-37.0 m CL1c (SPT N = 5-15)	23.0	32	0.30	19.6	18.48 ——— 18.74	0	0.90
37.0-42.0 m SM (SPT N = 12-34)	20.0	37	0.30	75.0	19.35 ——— 20.03	1	0.90
42.0-45.0 m CL2 (SPT N = 8-18)	25.0	35	0.30	15.7	18.62 ——— 18.91	5	0.90
45.0-48.0 m GC-GM (SPT N > 100)	30.0	39	0.30	270	20.75 ——— 22.08	2	0.95
> 48 m SS (SPT N > 100)	79.4	45	0.25	680	20.57 ——— 20.64	0	0.95
Testing Pile	Length L_p (m)	Diameter D_p (m)	Poisson's ratio ν_p	Young's modulus E_p (MPa)	Unit weight γ_p (kN/m^3)	-	
P39	70.7	2.0	0.19	33000	23.5	-	
P241	72.8	1.5	0.19	33000	23.5	-	

*R_{inter}: The strength reduction factor for the interface between the embedded pile and the soil. $c_{interface} = R_{inter} \times c_{soil}$, $\phi_{interface} = tan^{-1}[R_{inter} \times tan\phi_{soil}]$
SF = Surface Fill; CL = Low Plasticity Clay; SM = Silty Sand; GC-GM = Clayey Gravel to Silty Gravel; SS = Sand Stone

began in 1987 at Delft University of Technology as an initiative of the Dutch Ministry of Public Works and Water Management (Rijkswaterstaat). Because of continuously growing activities, the PLAXIS Company (Plaxis bv) was formed in 1993.

II. PILE LOADING TEST SIMULATION AND PARAMETRIC STUDY SETUP

In *Taipei 101* Construction Project (or *Taipei 101*), five pile loading tests (three extension piles and two compression piles) were carried out at the initial design stage. In this study, those test results were used to validate the suitability and reliability of numerical procedures and input material parameters via comparisons of pile settlements and load transfer curves between numerical simulations and measurements of pile loading tests. In the simulation, the soil was simulated by Mohr-Coulomb model and the pile was modeled by the embedded pile element. The capacity of the embedded pile to model the behavior of piled raft systems was discussed in Lee et al. (2010). The soil strata and properties of *Taipei 101* jobsite (Lin and Woo, 2000; 2005) were used for the simulation. However, the Young's modulii of soil layers were determined through a back analysis of pile loading testing data of *Taipei 101*. Input material model parameters in the simulation are listed in Table 1. In addition, the properties of pile-soil interface is considered using the strength reduction factor (R_{inter}) and the strength parameters of the interface $c_{interface}$ and $\phi_{interface}$ are calculated by $c_{interface} = R_{inter} \times c_{soil}$ and $\phi_{interface} = tan^{-1}[R_{inter} \times tan\phi_{soil}]$ respectively. The interaction behavior between pile and soil is affected by the properties of the interface. As a consequence, the R_{inter} value is calibrated through the comparison of numerical results and measurements of the pile loading tests first and subsequently

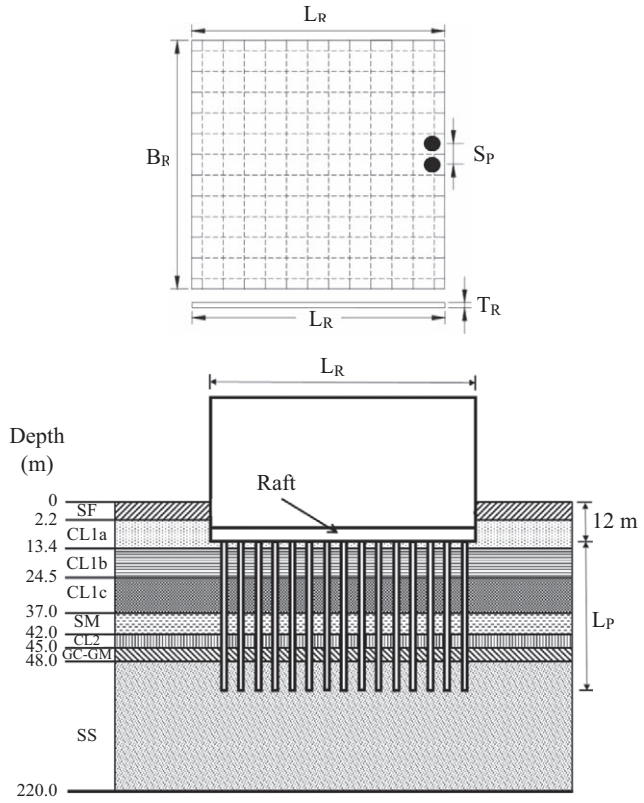

Fig. 1. Top and side view of the piled-raft foundation.

used in the sequential parametric studies. Simulation results indicated that the embedded pile element incorporating with the Mohr-Coulomb soil model can capture the behavior of the pile. As a consequence, the numerical procedures and input model parameters are verified and valid to use in the following parametric study. The detailed pile loading test simulation was discussed in Lin et al. (2016b).

The top and side views of the piled-raft foundation model used in the parametric study are shown in Fig. 1. In this study, the deep excavation with the excavation depth of 12 m and the diaphragm wall are both included in the simulation phases. The length, width and thickness of the raft and the spacing of piles are denoted as L_R, B_R, T_R and S_p respectively (as shown in Fig. 1). The distance from outskirt pile to raft edge is kept as 2 m. The finite element mesh of numerical model is shown in Fig. 2. The length, width and depth of the numerical model are 220 m × 220 m × 220 m. The left and right boundaries of the model are extended at least 4 times of the excavation depth (12 m) from the left and right edges of the raft foundation. The bottom boundary is extended at least 2.5 times of the longest pile length (= L_P = 55 m) from the pile tip. These dimensions are considered adequate to eliminate the influence of boundary effects on the interaction behaviors of the pile and diaphragm wall.

In the simulation of piled-raft foundation, the input parameters of soil layers are listed in Table 1. The excavation supporting structures of the numerical model include diaphragm

Table 2. Input model parameters of supporting structures and pile.

Supporting Structure	Diaphragm Wall	Floor Slab	Raft	H-Beam	Pile
Thickness t (m)	1.2	0.38	1.0	---	---
Cross section area A (m^2)	---	---	---	0.0219	3.142
Diameter D (m)	---	---	---	---	2.0
Unit Weight γ (kN/m^3)	23.5	23.5	23.52	76.94	24.09
Young's Modulus E (MPa)	25100	25100	33000	2×10^5	36000
Poisson ratio ν	0.15	0.15	0.15	---	---
Moment of inertia I ($\times 10^{-3}$ m^4)	---	---	---	I_x = 6.66 I_y =2.24	I_x =785 I_y =785

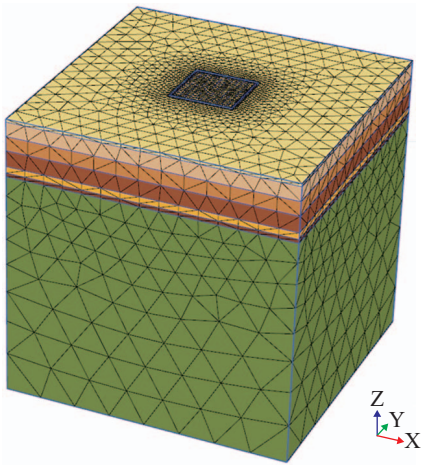

Fig. 2. Finite element mesh of numerical model.

wall, floor slab, H-beam (columns of floor), and raft foundation. Diaphragm wall, floor slab and raft foundation are modeled using plate element while H-Beam by beam element. Mechanical behaviors of these supporting structures are assumed to be linear elastic and isotropic. Material model parameters of supporting structures are summarized in Table 2.

The construction sequences for each calculation case are mainly simulated by following phases:

(1) Phase 1
Generate initial stress
(2) Phase 2
Install diaphragm wall, floor columns (using H-beam for construction) and piles for the piled-raft foundation
(3) Phase 3
Excavate to a depth of 12 m and install raft foundation
(4) Phase 4
apply structure loading to the piled-raft foundation. The structure loading is simulated by three typical loading intensities (3-story, 6-story, 9-story, 12-story of the superstructure) of residential building suggested by Liang et al. (2003).

Table 3. Setting of simulation cases in the parametric study.

Factor	Parametric Study Case Setting
RSF	*RSF* = 1.00 (B_R/L_R = 48 m/48 m), *PAF* = 2, *PSF* = 17.5 and T_R = 1 m
	RSF = 0.67 (B_R/L_R = 48 m/72 m), *PAF* = 2, *PSF* = 17.5 and T_R = 1 m
	RSF = 0.40 (B_R/L_R = 48 m/120 m), *PAF* = 2, *PSF* = 17.5 and T_R = 1 m
PAF	*PAF* = 2 (S_P/D_P = 4 m/2 m, 144 piles), (B_R/L_R = 48 m/48 m) *RSF* = 1.0, *PSF* = 17.5 and T_R = 1 m
	PAF = 3 (S_P/D_P = 6 m/2 m, 64 piles), (B_R/L_R = 48 m/48 m) *RSF* = 1.0, *PSF* = 17.5 and T_R = 1 m
	PAF = 4 (S_P/D_P = 8 m/2 m, 36 piles), (B_R/L_R = 48 m/48 m) *RSF* = 1.0, *PSF* = 17.5 and T_R = 1 m
PSF	*PSF* = 17.5 (L_P/D_P = 35 m/2 m), *RSF* = 1.0, *PAF* = 2 and T_R = 1 m
	PSF = 22.5 (L_P/D_P = 45 m/2 m), *RSF* = 1.0, *PAF* = 2 and T_R = 1 m
	PSF = 27.5 (L_P/D_P = 55 m/2 m), *RSF* = 1.0, *PAF* = 2 and T_R = 1 m
T_R	T_R = 1 m, *RSF* = 1.0, *PAF* = 2 and *PSF* = 17.5
	T_R = 2 m, *RSF* = 1.0, *PAF* = 2 and *PSF* = 17.5
	T_R = 3 m, *RSF* = 1.0, *PAF* = 2 and *PSF* = 17.5

The loading intensities of 3-story, 6-story, 9-story, 12-story of the superstructure are 98.56 kN/m^2, 147.8 kN/m^2, 197.1 kN/m^2, and 246.4 kN/m^2 respectively. The detail model simulation procedures of entire construction stages consist of 11 simulation phases and can be referred to the research work of Chen (2014). In the following sections the numerical results of the piled-raft foundation in *Phase 4* with the loading intensity of the 12-story superstructure are discussed.

From previous studies (Kahyaoglu et al., 2009; Lee et al., 2010; Huang et al., 2011; Cho, 2012; Nguyen et al., 2013), pile lengths (length/diameter ratio), pile configurations (pile number, spacing/diameter ratio), raft and pile characteristics, and soil parameters are founded to have significant effects on the interaction behaviors of the piled-raft foundation. In this study, a typical soil strata and soil parameters of Taipei Metropolitan were adopted throughout the analyses. Conclusively, four most important influence factors were selected for the subsequent parametric study to investigate their effects on the raft settlement, the pile head loading, the pile bending moment and the load carrying ratio of the piled-raft foundation. The four influence factors can be depicted as follows:

(1) *Raft Size Factor* (*RSF*)
RSF defines the shape (square or rectangular) of the piled-raft foundation. *RSF* equals to the raft width divided by the raft length (B_R/L_R).

(2) *Pile Arrangement Factor* (*PAF*)
PAF equals to the pile spacing divided by the pile diameter (S_P/D_P). In the numerical investigation of *PAF* factor, the raft dimension B_R and L_R are specified to be identical (B_R = L_R = 48 m or B_R/L_R = 1.0). Therefore, *PAF* is used to represent the arrangement and the number of pile in the pile group of piled-raft foundation.

(3) *Pile Size Factor* (*PSF*)
PSF described the length of the pile installed in the piled-raft foundation. *PSF* equals to the pile length divided by the pile diameter (L_P/D_P).

(4) *Raft Thickness* (T_R)
T_R is the thickness of the raft.

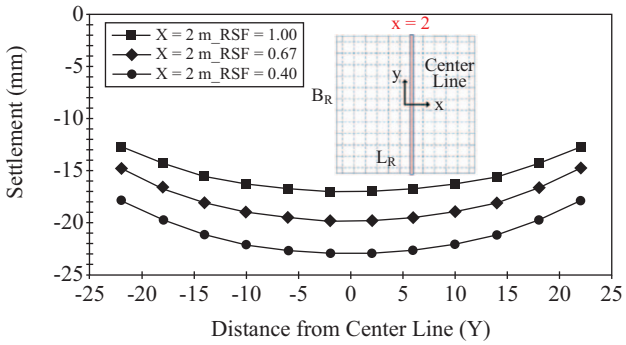

Fig. 3. The settlement of piled-raft for different RSF values.

The simulation cases adopted in this study are listed in Table 3 and simulation results are discussed in the following sections.

III. PARAMETRIC STUDY RESULTS

1. Influence of Factor *RSF* (= B_R/L_R)

Since the piled-raft foundation settlement profile along the section of X = 2 m (see Fig. 3) displays a maximum value of settlement when subjected to a vertical loading from superstructure, it was therefore selected for a representative and further discussion. As illustrated in Fig. 3, the settlement pattern of the piled-raft foundation for different cases of *RSF* (= B_R/L_R = 1.0, 0.67 and 0.40) constantly showed a concave shape pattern and which is similar to the patterns observed from previous studies (Poulos et al., 1997; Comodromos et al., 2009; Lee et al., 2010; Poulos et al., 2011; Lin et al., 2016a). The piled-raft foundation settlement increases as the raft geometry changes from square shape (*RSF* = 1.0) to rectangular shape (*RSF* = 0.4). The maximum settlements (or δ_{vmax} value) of the piled-raft foundation subjected to a vertical uniform loading of 12-story building for *RSF* = 1.0, 0.67 and 0.4 are equivalent to 17.02, 19.82, 22.93 mm respectively. However, it should be pointed out that for the different cases of *RSF* (= B_R/L_R), the corresponding numbers of piles in pile group are 144 piles (= 12 × 12 for *RSF* = 1.0), 216 piles (= 12 × 18 for *RSF* = 0.67) and 360 piles (= 12 × 30 for *RSF* = 0.40) when *PAF* (= S_p/D_p = 2) is constant as listed in Table 3. As shown in Fig. 3, the raft settlement profile of rectangular shape is greater than that of square shape although the rectangular shape possesses a larger number of piles in pile group. This also implies that the raft shape dominates the raft settlement

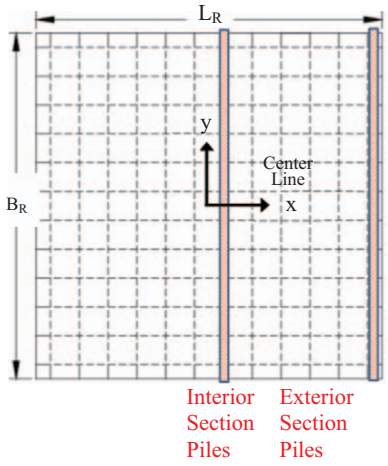

Fig. 4. Sections selected for the load distribution on pile head.

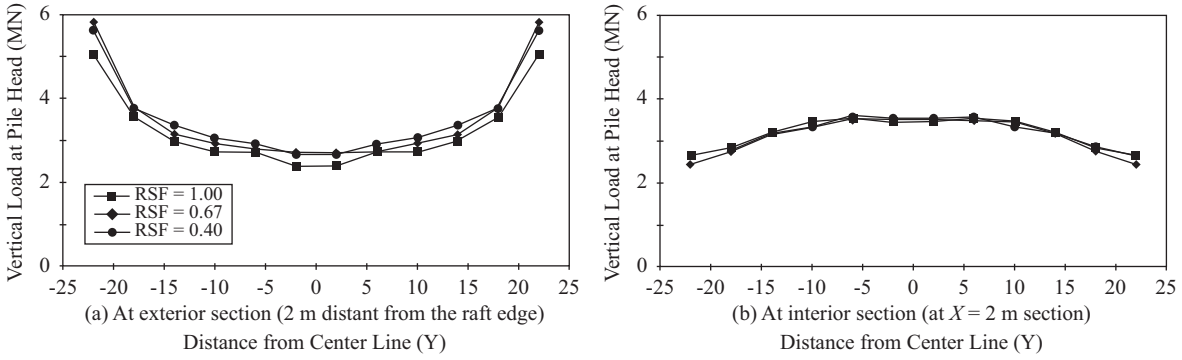

Fig. 5. Pile head load distribution for different RSF values.

of the piled-raft rather than the number of pile. In addition, another adverse effect on the case of smaller *RSF* value with larger number of piles is the stress overlapping in the soil strata due to heavily load transferred from the pile shaft to the soil strata at the central area of pile group.

For the pile head load, piles at the exterior section and the interior section are selected for the discussion (see Fig. 4) because these two sections represent two types of pile head load distributions. The exterior section has higher pile head loads in edge piles and lower pile head loads in center piles. On the other hand, the interior section has higher pile loads in center piles and lower pile loads in edge piles. Conclusively, the maximum pile head load occurs at corners of the piled-raft foundation. Pile load measurements of the Messe-Torhaus in Frankfurt presented in Small and Poulos (2007) and numerical simulation results in Bourgeois et al. (2012) and Lin et al. (2016a) show an identical load distribution pattern. As shown in Fig. 5, the pile head load distributions along both the exterior and interior sections for different *RSF* cases are very similar even though there exists a large difference in the pile number. Conclusively, the maximum loads carried by piles are 5.05 MN for *RSF* = 1.0 with pile number of 144 piles, 5.81 MN for *RSF* = 0.67 with pile number of 216 piles and 5.62 MN for *RSF* = 0.4 with pile number of 360 piles.

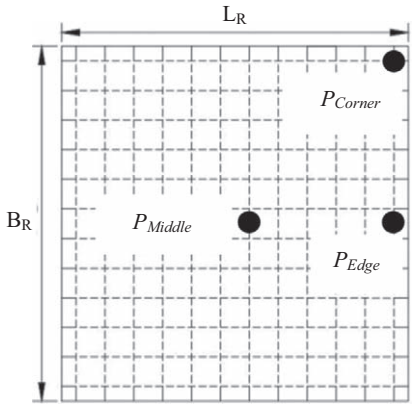

Fig. 6. Locations of selected piles for the comparison of bending moment.

For the pile bending moment, three piles, namely, the corner pile (P_{Corner}), edge pile (P_{Edge}) and middle pile (P_{Middle}) are selected because of their different load carrying and settlement conditions (see Fig. 6). Fig. 7 exhibits the bending moments of three selected piles. Edge pile (P_{Edge}) has higher bend moments along the pile shaft because the raft edge was curved due to a vertical uniform loading of building. The up-curved defor-

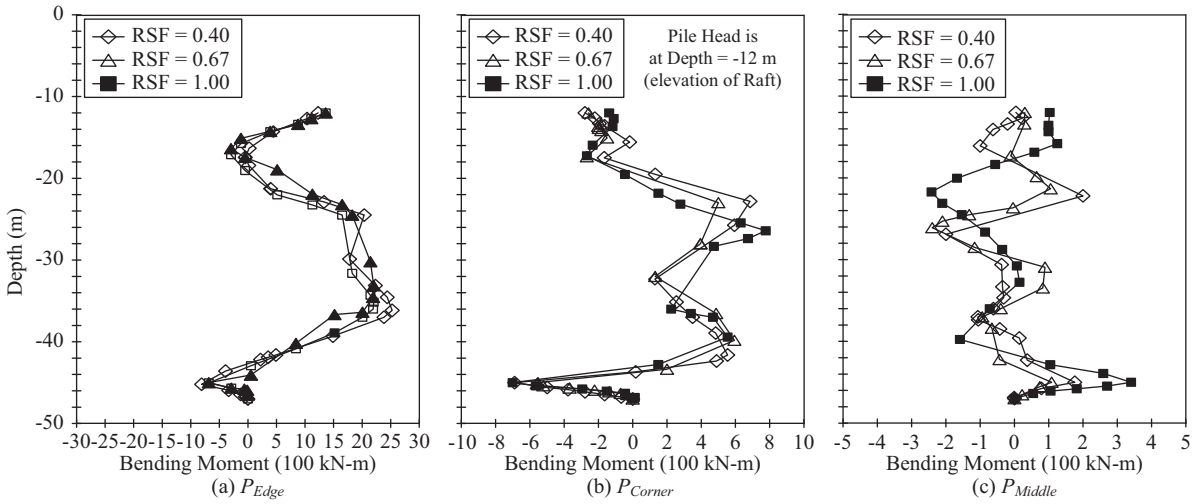

Fig. 7. Bending moments of piles for different RSF values.

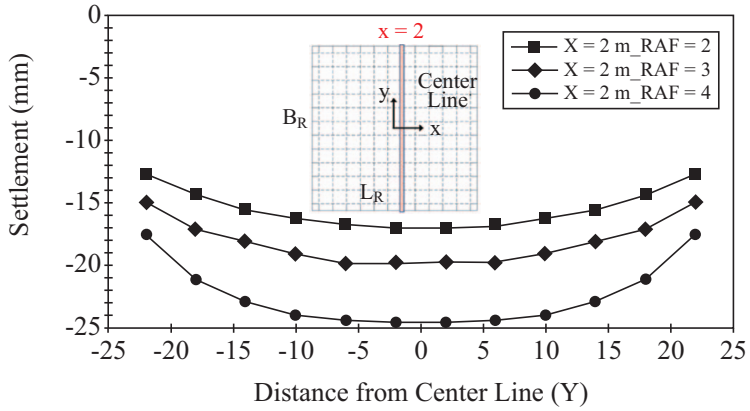

Fig. 8. The settlement of piled-raft for different PAF values.

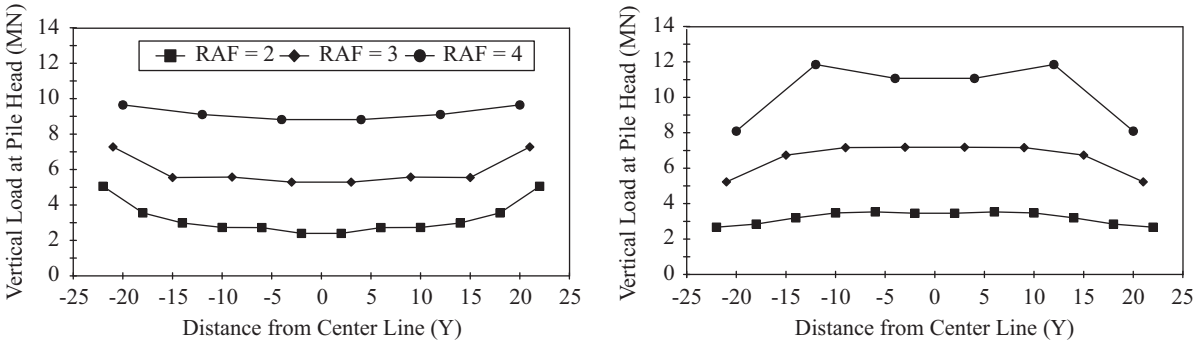

Fig. 9. Pile head load distribution for different *PAF* values.

mation at raft edge alternately causes a large lateral displacements at the pile head of P_{Edge}. The bending moment patterns are identical with those observed in Lin et al. (2016a). In general, the *RSF* has no significant influence on the bending moment of pile shaft.

2. Influence of Factor *PAF* (= S_P/D_P)

As shown in Fig 8, the settlement of piled-raft observably reduces with a decreasing *PAF* value which accompanied with a smaller pile spacing and larger number of piles. The maximum

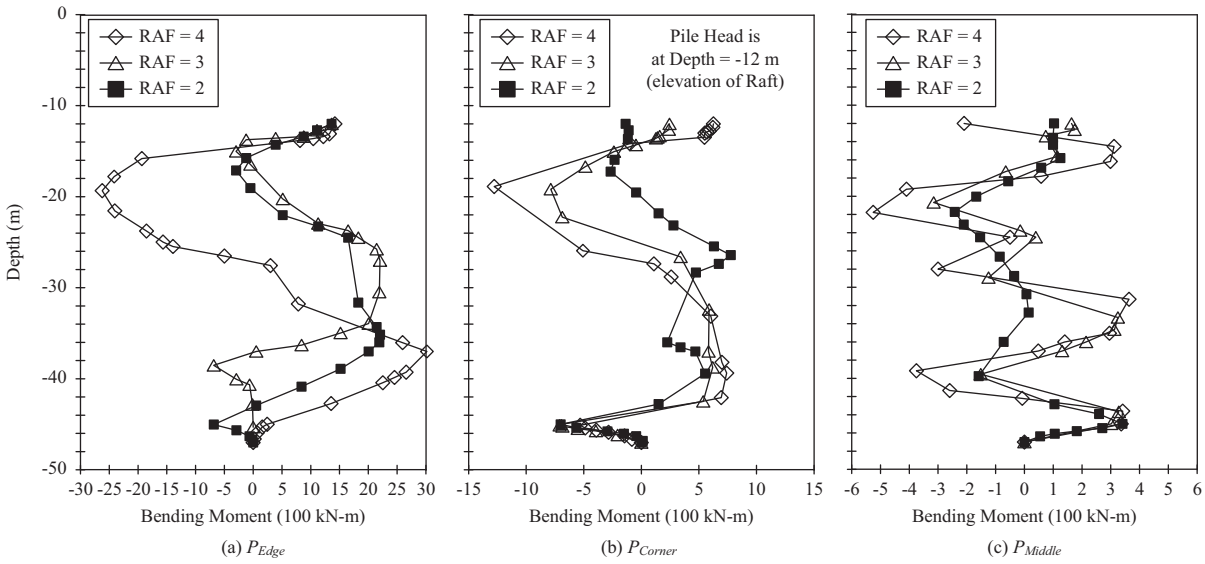

Fig. 10. Bending moments of piles for different *PAF* values.

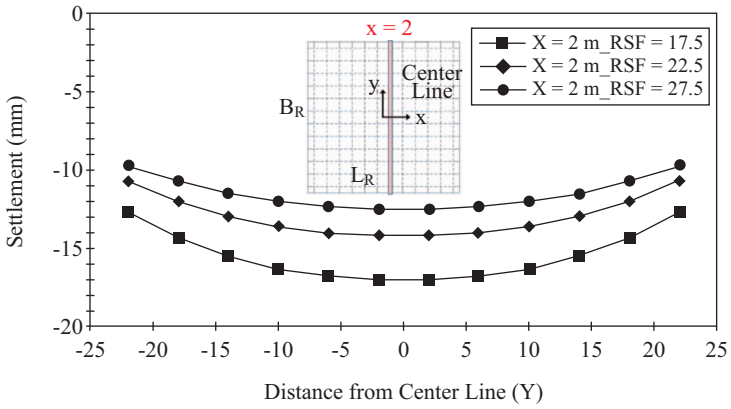

Fig. 11. Settlement of piled raft for different *PSF* values.

settlements of piled-raft subjected to a vertical uniform loading of 12-story building for *PAF* = 2, 3 and 4 (*PAF* = 2 → 4 represents pile spacing increased while pile number decreased) are 17.02, 19.85 and 24.59 mm respectively.

The pile head load distribution patterns, as shown in Fig. 9, are fairly similar and piles with a larger *PAF* value carry higher vertical loads due to the loading is shared by fewer piles. The maximum loads at pile head are 5.05 MN for *PAF* = 2, 7.28 MN for *PAF* = 3 and 11.85 MN for *PAF* = 4.

Fig. 10 illustrates that the edge pile (P_{Edge}) exhibits a higher bending moment along the pile shaft because the raft edge was curved due to vertical loading and which subsequently imposes a large lateral displacement on pile head. The effects of *PAF* on the bending moment of the piles are dependent on the pile location. The *PAF* only has a slight influence on middle pile (P_{Middle}) but a significant influence on corner pile P_{Corner} and edge pile P_{Edge}. The reason is that the lateral displacements at the corner and the edge of the raft are larger for a condition with larger *PAF* and this large lateral displacement can lead to a significant increase of the bending moment.

3. Influence of Factor *PSF* (= L_P/D_P)

According to Fig. 11, the magnitude of the piled-raft foundation settlement decreases as the *PSF* value increases (longer pile length). The main reason is that a pile merely needs a less relative movement (less than the piled-raft settlement) at interface between the pile and the soil to mobilize the full frictional resistance to support the vertical loading transmitted from piled-raft foundation. Therefore, the magnitude of the settlement decreases as the pile length increases. The maximum raft settlements of piled raft subjected to a 12-story vertical uniform loading for *PSF* = 17.5, 22.5 and 27.5 are 17.02, 14.19 and 12.51 mm respectively.

The pile head load distribution for different *PSF* cases, as shown in Fig. 12, has an identical pattern and the magnitude of

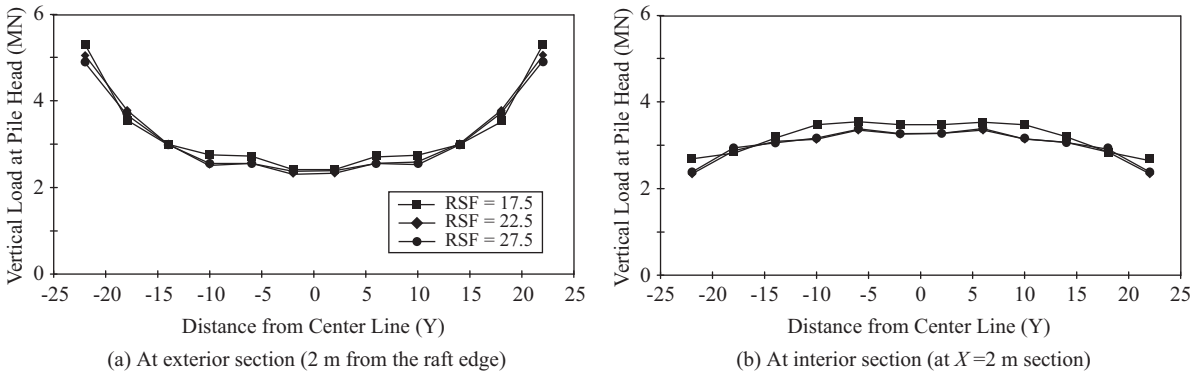

Fig. 12. Pile head load distribution for different *PSF* values.

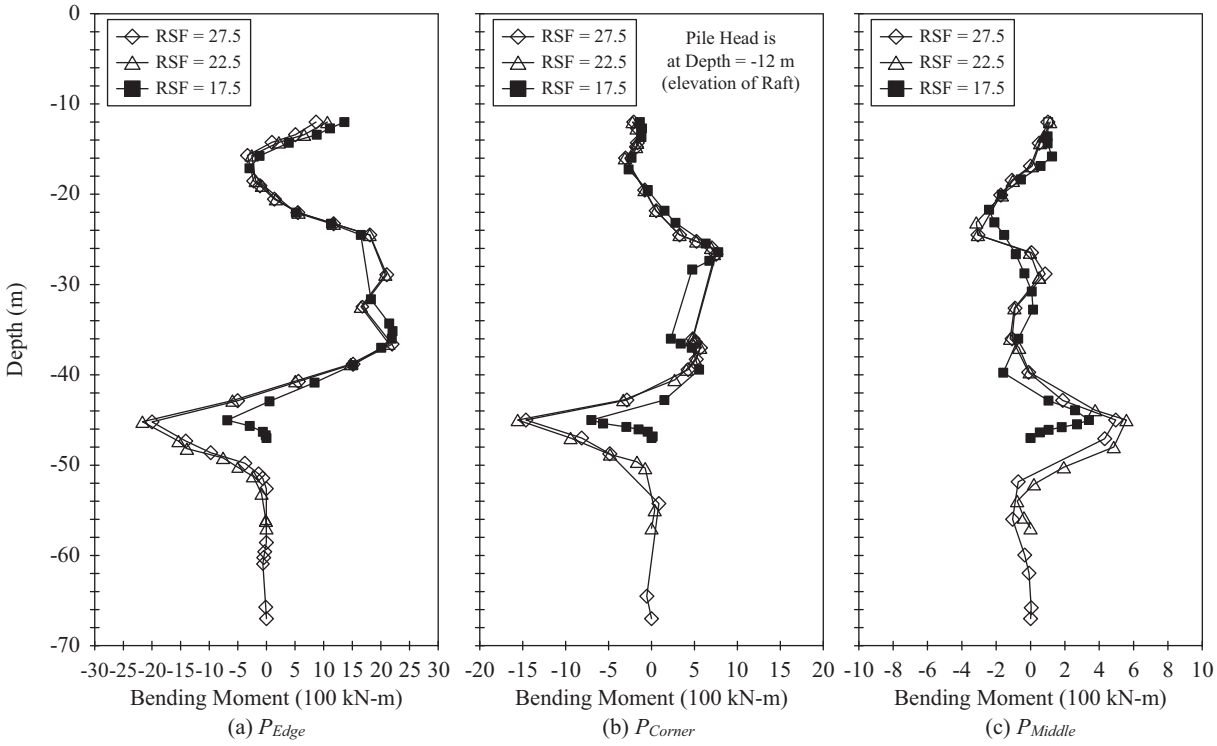

Fig. 13. Bending moments of piles for different *PSF* values.

loads carried by piles are similar. This is because of the effect of *PSF* value on the pile group for vertical loading only reflects on the pile length rather than the number of piles. The maximum loads of piles are 5.28 MN for *PSF* = 17.5, 5.05 MN for *PSF* = 22.5 and 4.98 MN for *PSF* = 27.5. The pile head load distributions for a piled-raft with larger *PSF* (= 27.5) value are slightly lower than those with smaller *PSF* values (= 17.5, 22.5) because of the raft with larger *PSF* value carries more vertical loading. In other words, under an identical loading condition, piles carry less loading in a larger *PSF* situation. However, numerical results indicated the *PSF* value merely exhibits minor effects on the pile head loading. Since the bearing layer (*S*and *S*tone layer or *SS* layer) located at a depth of 48 m from ground surface, for a typical deep excavation with excavation depth of 12 m, the penetration depth of pile into bearing layer for *PSF* = 17.5, 22.5 and 27.5 are 0.0 (= 0.0 D_P), 9.0 (= 4.5 D_P) and 19.0 m (= 9.5 D_P) respectively. Accordingly, considering the engineering cost and efficiency of pile group, it is suggested that a proper penetration depth of pile into *SS* layer should be in a range of 2-3 D_P (= 4-6 m).

As shown in Fig. 13, the pile shaft adjacent to the *S*and *S*tone (*SS*) layer (at a depth of 48 m from ground surface) undergoes a higher bending moment when the pile was penetrated into the *SS* layer and accompanied with a constraint effect imposed by

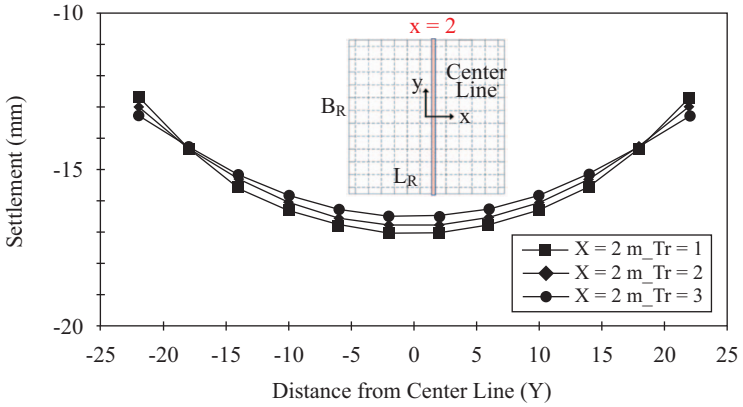

Fig. 14. The settlement of piled raft for different T_R values.

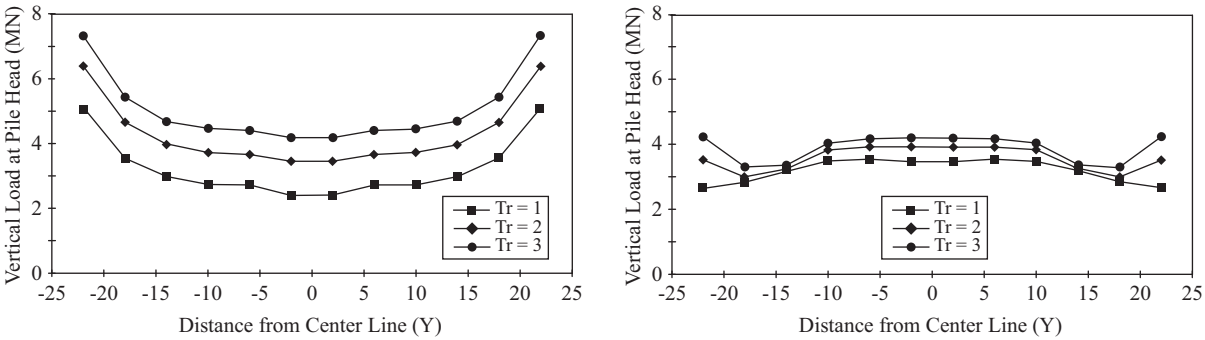

Fig. 15. Pile head load distribution for different T_R values.

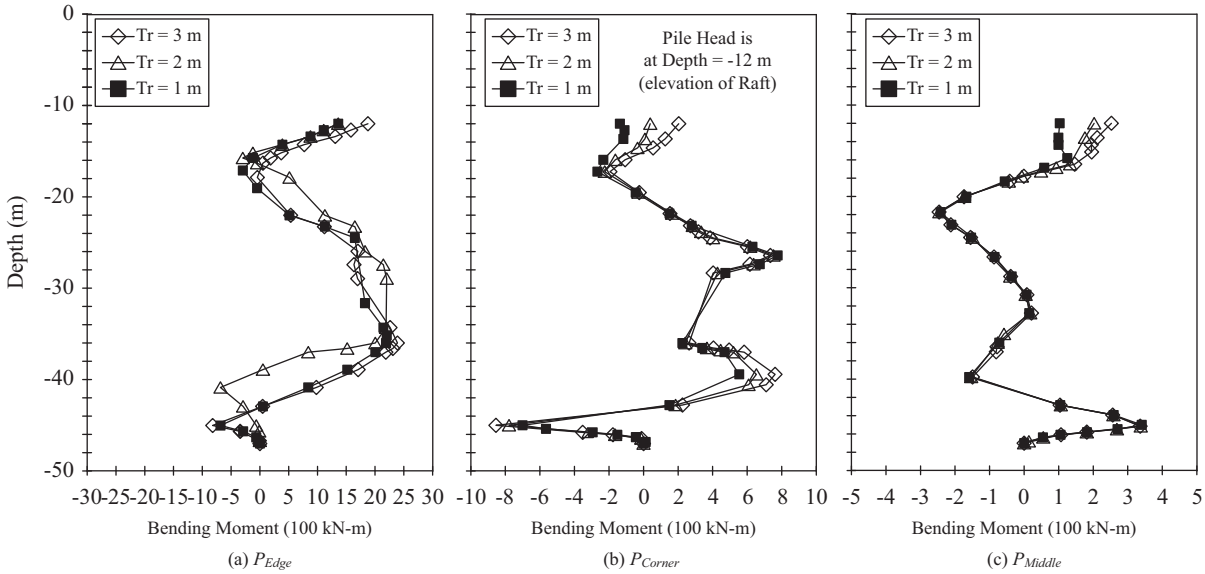

Fig. 16. Bending moments of piles for different T_R values.

the stiff *SS* layer on the pile tip. Moreover, as explained in the above paragraph, the lateral displacement of corner pile P_{Corner} is larger than those of edge pile P_{Edge} and middle pile P_{Middle} because the raft edge was curved by vertical loading and which alternately imposed a large lateral displacement on pile head. This large lateral displacement can lead to a significant increment

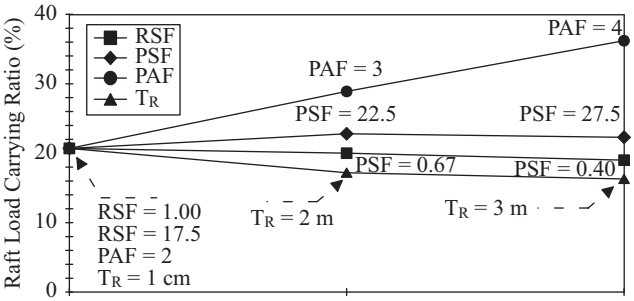

Fig. 17. *LCR* values for the variation of different influence factors.

of bending moment of corner pile P_{Corner} at the depth adjacent to the *S*and *S*tone (*SS*) layer.

4. Influence of Factor T_R

Fig. 14 shows the settlement of the piled-raft foundation for different raft thickness T_R (= 1, 2 and 3 m). In general, the raft thickness T_R for a common multi-floor building is about in a range of 0.7-1.2 m except for a high rise building such as *Taipei 101* using a raft thickness of 3 m. The raft settlement is smaller for a thicker raft due to the fact of a higher flexural stiffness provided by a larger cross sectional area of raft. However, the raft thickness only has a minor effect on the raft settlement. In addition, as expected, a thicker raft can mitigate the differential settlement of the raft. This behavior was also observed in several researches (Oh et al., 2009; Rabiei, 2009; El-Garhy, 2013 and Lin et al., 2016a). The maximum settlements of piled-raft subjected to a vertical uniform loading of 12-story building are 17.02, 16.80 and 16.50 mm for raft thickness T_R=1, 2 and 3 m respectively.

The pile head load distribution for different T_R cases, as shown in Fig. 15, has an identical distribution pattern but the piles with a thicker raft carry larger loads. Although a thicker raft enables to reduce the total settlement and differential settlement of piled-raft, the pile head loading increases due to carrying more self-weight surcharge resulted from a thicker raft. In conclusion, the pile needs to carry more loading in case of a thicker raft. The maximum loads of piles are 5.05 MN for T_R = 1 m, 6.39 MN for T_R = 2 m and 7.32 MN for T_R = 3 m.

As illustrated in Fig. 14, the raft thickness T_R only has a slight effect on the raft settlement. On the other hand, the pile bending moment is significantly related to the pattern and magnitude of raft settlement as shown in Figs. 8 and 10 (or Figs. 3 and 7). As a consequence, the bending moments of piles at different locations of raft P_{Corner}, P_{Edge} and P_{Middle} are insensitive to the raft thickness T_R and the distribution pattern and the magnitude of bending moments for each individual pile such as at corner, edge and middle are similar, as shown in Fig. 16.

5. Raft Contribution to the Bearing Capacity of Piled-Raft

In the conventional design of the piled-raft foundation, a conservative design concept ignoring the bearing effect of raft is commonly adopted to ensure the effective function and high safety of the pile group. However, this conservative design makes the piled-raft foundation less economical. Recent studies on real case histories and full scale pile group tests (Liang et al., 2003; Lee et al., 2010; Long, 2010) demonstrated that the raft can carry 15% to 70% of the total load. In this study, a *L*oad *C*arrying *R*atio (*LCR*) was used to calculate the contribution percentage of the total load carrying by the raft. The *LCR* can be calculated as follows:

$$LCR = Q_R / Q_T \quad \text{and} \quad Q_R = Q_T - \sum_{i=1}^{n} Q_{Pi}$$

where *LCR* is the load carrying ratio of the raft; Q_T is the total load carried by the piled-raft foundation; Q_R is the load carried by the raft; Q_{Pi} is the load carried by the i^{th}-pile (i = 1-n, n = the total number of pile in pile group). As shown in Fig. 17, *PAF* (= S_P/D_P = pile spacing/pile diameter) demonstrates significant effects on the *LCR* whereas other influence factors *PSF* (= L_P/D_P = pile length/pile diameter), *RSF* (= B_R/L_R = raft width/raft length) and T_R (raft thickness) only exhibit minor effects on the *LCR*. In general, a higher *LCR* value is usually associated with a larger settlement of the piled-raft foundation because a larger portion of vertical loading is transferred to the foundation soil strata underneath the raft via the raft settlement, especially for a piled-raft with higher *PAF* value (fewer piles in pile group). This loading transfer mechanism was also found in the centrifuge testing results (Lee et al., 2010). In this study, the raft carries about 20% to 35% of the total vertical load on the piled-raft system of deep excavation in Taipei Metropolitan. However, it should be pointed out that in case of subsiding environment with end bearing piles, the raft contribution to load carrying has to be accounted for only after careful consideration.

IV. CONCLUSIONS

The piled-raft foundation is often used to solve the low bearing capacity of the soil and the excess settlement problem of the raft foundation. In this article, a parametric study on piled-raft system considering the deep excavation, the installation of the diaphragm wall and the overburden stress of the surrounding soil was performed to investigate the effects of four influence factors (*RSF*, *PAF*, *PSF* and T_R) on the vertical load transfer behaviors of piled-raft foundation in the typical soil strata of Taipei Metropolitan. The 3-D FEM numerical procedures and material model parameters used in this study were firstly calibrated and validated using pile loading test results in the jobsite of *Taipei 101*. Subsequently, a series of parametric studies were performed using the four influence factors as numerical variables. According to the numerical results, several conclusions are made as follows:

(1) *Raft Size Factor* (*RSF* = L_R/B_R = 1.0, 0.67, and 0.4)
The raft settlement decreases as *RSF* increases from 0.4 (a rectangular raft) to 1.0 (a square raft). *RSF* only has minor

effects on the pile head loading, the pile bending moment and the load carrying ratio of raft (*LCR*).

(2) *Pile Arrangement Factor* ($PAF = S_P/D_P = 2$, 3, and 4)
A higher *PAF* value denotes less number of piles are installed in the piled-raft foundation. The raft settlement, the pile head loading, the pile bending moment and *LCR* all increase with an increasing *PAF* value.

(3) *Pile Size Factor* ($PSF = L_P/D_P = 17.5$, 22.5, 27.5)
A larger *PSF* value represents piles with longer length are installed in the piled-raft foundation. The raft settlement reduces with an increasing *PSF* value whereas the *PSF* value merely exhibits minor effects on the pile head loading and *LCR*. For a larger *PSF* value (longer pile length), the pile shaft adjacent to the top of *S*and *S*tone (*SS*) layer (at a depth of 48 m from ground surface) undergoes a higher bending moment when the pile was penetrated into the *SS* layer which imposed a constraint effect on the pile tip. For a typical deep excavation with excavation depth of 12 m, 3-floor basement, and 12-story superstructure in Taipei Metropolitan, it is suggested that a penetration depth of pile into *S*and *S*tone layer (or bearing layer in Taipei subsoil) equals to 2 to 3 D_P should be proper for engineering practices.

(4) *Raft Thickness* ($T_R = 1$, 2, and 3 m)
The raft settlement and differential settlement decrease with an increasing T_R value due to a higher flexural stiffness provided by a thicker raft. The pile head loading increases with an increasing T_R value because of a larger self-weight surcharge resulted from a thicker raft. However, the influence of T_R value on the pile bending moment is insignificant.

(5) *L*oad *C*arrying *R*atio of raft ($LCR = Q_R/Q_T$)
LCR of raft is greatly relevant to the raft settlement. A higher *LCR* value is constantly associated with a larger settlement of piled-raft because a larger portion of vertical loading is transferred to the foundation soil strata underneath the raft via the raft settlement, especially for the piled-raft with a larger *PAF* value (or fewer piles in pile group). In this study, the raft carries 20% to 35% of the total vertical load on the piled-raft system of deep excavation in Taipei Metropolitan. Conclusively, under a condition of satisfying the requirement of allowable total settlement and differential settlement of raft, the number of pile and engineering cost can be largely curtailed if the *LCR* of raft is taken into account in the conventional design procedures of piled-raft system.

REFERENCES

Bourgeois, E., P. De Buhan and G. Hassen (2012). Settlement analysis of piled-raft foundations by means of a multiphase model accounting for soil-pile interactions. Computers and Geotechnics 46, 26-38.

Chen, S. Y. (2014). Three-dimensional analysis of piled-raft foundation in deep excavation of Taipei Metropolitan. Master Thesis, Department of Soil and Water Conservation, National Chung-Hsing University

Clancy, P. and M. F. Randolf (1993). An approximate analysis procedure for piled raft foundations. International Journal for Numerical Methods in Geomechanics 17, 849-869.

Comodromos, E. M., M. C. Papadopoulou and I. K. Rentzeperis (2009). Pile foundation analysis and design using experimental data and 3-D numerical analysis. Computers and Geotechnics 36(5), 819-836.

Nguyen, D. D. C., S. B. Jo and D. S. Kim (2013). Design method of piled-raft foundations under vertical load considering interaction effects. Computers and Geotechnics 47, 16-27.

El-Garhy, B., A. A. Galil, A. F. Youssef and M. A. Raia (2013). Behavior of raft on settlement reducing piles: Experimental model study. Journal of Rock Mechanics and Geotechnical Engineering 5(5), 389-399.

Cho, J., J. H. Lee, S. Jeong and J. Lee (2012). The settlement behavior of piled raft in clay soils. Ocean Engineering 53, 153-163

Lee, J., Y. Kim and S. Jeong (2010).Three-dimensional analysis of bearing behavior of piled raft on soft clay. Computers and Geotechnics 37, 103-114.

Karim, H. H., M. R. AL-Qaissy and M. K. Hameedi (2013). Numerical analysis of piled raft foundation on clayey soil. Eng. & Tech. Journal Part (A) 31(7), 1297-1312.

Lee, S. W., W. W. L. Cheang, W. M. Swolfs and R. B. J. Brinkgreve (2010). Modelling of piled rafts with different pile models. In Proceedings of the 7th European Conference on Numerical Methods in Geotechnical Engineering. Trondheim, Norway: CRC Press (637-642).

Liang, F. Y., L. Z. Chen and X. G. Shi (2003). Numerical analysis of composite piled raft with cushion subjected to vertical load. Computers and Geotechnics 30(6), 443-453.

Lin, D. G., W. T. Liu and J. C. Chou (2016a). Load transfer and deformation analyses of piled-raft foundation in Taipei Metropolitan. Journal of Marine Science and Technology 24(4), 786-794.

Lin, D. G., W. T. Liu and J. C. Chou (2016b). Mechanical behaviors of piled-raft foundation and diaphragm wall in deep excavation of Taipei Metropolitan. Journal of Marine Science and Technology 24(5), 980-991.

Lin, D.G. and S. M. Woo (2000). Deformation analysis of Taipei International Financial Center deep excavation project, technical report. Trinity Foundation Engineering Consultants Co., LTD.

Lin, D. G. and S. M. Woo (2005). Geotechnical analyses of Taipei International Financial Center (Taipei 101) Construction Project, 16th International Conference on Soil Mechanics and Geotechnical Engineering, 1513-1516, September 12-16, 2005, Osaka, Japan.

Long, P. D. (2010). Piled raft-a cost-effective foundation method for high-rises. Geotechnical Engineering 41(3), 1-12.

Huang, M., F. Liang and J. Jiang (2011). A simplified nonlinear analysis method for piled raft foundation in layered soils under vertical loading. Computers and Geotechnics 38, 875-882.

Kahyaoglu, M. R., G. Imancli, A. U. Ozturk and A. S. Kayalar (2009). Computational 3D finite element analyses of model passive piles. Computational Materials Science 46(1), 193-202.

Nguyen, D. D. C., D. S. Kim and S. B. Jo (2014). Parametric study for optimal design of large piled raft foundations on sand. Computers and Geotechnics 55, 14-26.

Oh, E. Y. N., Q. M. Bui, C. Surarak and A. S. Balasurbamaniam (2009). Investigation of the behavior of piled raft foundations in sand by numerical modeling. In The Nineteenth International Offshore and Polar Engineering Conference. International Society of Offshore and Polar Engineers.

Poulos, H. G. (1991). Analysis of piled strip foundations. Computer Methods and Advances in Geomechanics (1), 183-191.

Poulos, H. G. (1994). An approximate numerical analysis of pile-raft interaction. International Journal for Numerical and Analytical Methods in Geomechanics 18(2), 73-92.

Poulos, H. G. and E. H. Davis (1980). Pile Foundation Analysis and Design. John Wiley and sons, New York.

Poulos, H. G., J. C. Small, L. D. Ta, J. Sinha and L. Chen (1997). Comparison of some methods for analysis of piled rafts. Proceedings of the 30th year symposium of the Southeast Asian Geotechnical Society 2, 1119-1124.

Poulos, H. G., J. C. Small and H. Chow(2011). Piled raft foundations for tall buildings. Geotechnical Engineering Journal of the SEAGS and AGSSEA 42(2), 78-84.

Rabiei, M. (2009). Parametric study for piled raft foundations. EJGE 14, 1-11.

Randolph, M. F. (1983). Design of Piled Raft Foundations. Cambridge University Engineering Department.

Randolph, M. F., R. Dolwin and R. Beck (1994). Design of driven piles in sand. Geotechnique 44(3), 427-448.

Small, J. C. and H. G. Poulos (2007). Nonlinear analysis of piled raft foundations. Contemporary Issues In Deep Foundations. ASCE, 1-9.